Proton beams from intense laser-solid interaction: effects of the target materials

Y. X. Geng,[1] D. Wu,[2,*] W. Yu,[3] Z. M. Sheng,[4,5] S. Fritzsche,[6] Q. Liao,[1] M. J. Wu,[1] X. H. Xu,[1] D. Y. Li,[1] W. J. Ma,[1] H. Y. Lu,[1] Y. Y. Zhao,[1] X. T. He,[1] J. E. Chen,[1] C. Lin,[1,†] and X. Q. Yan[1,‡]

[1]*Key Laboratory of HEDP of the Ministry of Education, CAPT, and State Key Laboratory of Nuclear Physics and Technology, Peking University, Beijing, 100871, China*
[2]*Institute for Fusion Theory and Simulation, Department of Physics, Zhejiang University, 310058 Hangzhou, China*
[3]*State Key Laboratory of High Field Laser Physics, Shanghai Institute of Optics and Fine Mechanics, 201800 Shanghai, China*
[4]*SUPA Department of Physics, University of Strathclyde, Glasgow, G4 0NG UK*
[5]*Key Laboratory for Laser Plasmas (Ministry of Education), School of Physics and Astronomy, Shanghai Jiao Tong University, Shanghai 200240, China*
[6]*Helmholtz Institut Jena and Friedrich-Schiller-University Jena, D-07743 Jena, Germany*

(Dated: September 11, 2019)

We report systematic studies of the laser-driven proton beams produced with micron-thick solid targets made of aluminum and plastic, respectively. Distinct effects of the target materials are found on the total charge, cut-off energies and spot sizes of protons in the experiments, which are well reveal by two dimensional particle-in-cell simulations including both ionization dynamics and collision dynamics for different material properties. It is found that with a laser intensity of 8×10^{19} W/cm^2, the target normal sheath acceleration is dominant for both targets. The higher charge and cut-off energy of the protons from the plastic targets are due to the higher energy coupling efficiencies from the intense laser beams. Large spot sizes of the protons from the plastic targets are due to the deflection of hot electrons when transporting in targets. The cut-off energies of protons are decreased when increasing the target thickness, and this is due to the energy loss of hot electrons when transporting in targets. The consistent results further narrow the gap between the simulation and the experiment in reality.

PACS numbers: 52.38.Kd, 41.75.Jv, 52.35.Mw, 52.59.-f

Introduction In the last few decades laser driven proton acceleration [1–4] has been explored widely because of its potential applications [5–10] in medicine, material processing, radiograph and high energy density physics. These beams often exhibit unique properties, such as high brightness, short duration and low emittance. One of the well-established and robust mechanisms for proton accelerations is the so-called target normal sheath acceleration [1]. In this mechanism, protons are accelerated from the target rear by a strong sheath electric field (TV/m) built by the expansion of intense energetic-electrons originally generated in front of the target and then transport through the target.

The investigations of the target materials on proton acceleration has been extensively studied in the past decades. For example, it was experimentally demonstrated that protons from the thin solid plastic targets were higher in cut-off energies and charge as compared with those generated from the aluminum targets, when irradiated by laser pulse with an intensity of $\sim 10^{18}$ W/cm^2 [11]. To explain the experiment result, an analytical model that include some material properties had been established, which suggests that the proton acceleration is enhanced by a resistively induced electric field in the front of the plastic target [11–13]. In the mean time, the transport of hot electrons within plastic target is significantly inhibited and filamented, consequently induces uniformity on the profile of the protons. It was observed in the experiments [14, 15] and then confirmed by a different concept of PIC code [16] based on a hierarchical N-body tree algorithm. The previous researches are successful in explaining each single aspect, for instance, why the proton beam from the plastic target has either high energy or a uniform spot.

However, in order to fully understand the effect of the target material properties on proton acceleration, a full simulation model shall include ionization dynamics [17, 18], collision dynamics [19, 20], degenerate plasmas states [21, 22] and collective electromagnetic fields [23–25], which is not available so far. Recently, a new particle-in-cell (PIC) code has been developed, which is based on high order implicit numerical scheme [26] and takes advantage of the newly developed ionization [27, 28] and collision [29] dynamics models. This code enables us to calculate coupled atomic and plasma processes for solid density targets in a more realistic way. Within the simulations, the ionization charge state and conductivity (or resistivity) of the target can self-consistent evolve precisely according to the local plasma and electromagnetic fields conditions. Different types of materials (single or alloys), such as aluminum and plastics, can now be modelled based on their intrinsic atomic properties.

In this Letter, the effects of target materials on laser-driven proton accelerations are investigated, where solid

* Email: dwu.phys@zju.edu.cn
† Email: lc0812@pku.edu.cn
‡ Email: xueqingyan@pku.edu.cn

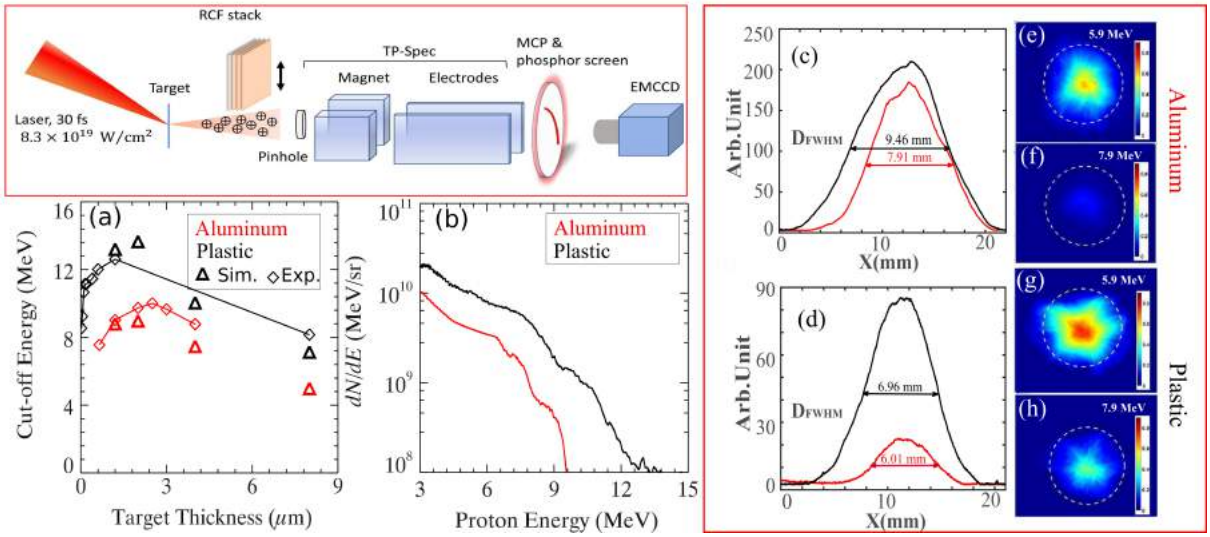

FIG. 1. (Top, left) Experimental setup. (a) The variation of the cut-off energy of protons with the target thickness. Here diamonds are from the 5 best shots average in experiments and triangles are from PIC simulations. (b) The optimum energy spectra of protons for aluminum and plastic targets detected by the Thomson spectrometer. (c)-(d) and (e)-(h) the energy-resolved spatial distributions of proton beams detected by the RCF stack for the 2.5 μm aluminum and the 1.2 μm plastic targets. The white circles indicate the position of protons with a deflection angle of 14°.

targets of aluminum and plastic with varying thickness are applied. Experimental measurements indicate that total charge and cut-off energies of the protons from the plastic targets are much higher than those from aluminum targets, and the proton beam from plastic targets has a uniform spot. Moreover, the cut-off energies of protons is decreased by furthering increasing of target thickness. These findings are well elucidated by the newly developed PIC simulation code.

Experimental setup The experiments were performed at the Laboratory for Compact LAser Plasma Accelerator (CLAPA) at Peking University. An $f/3.5$ off-axis parabola (OAP) mirror was used to focus the 30 fs duration and 800 nm wavelength pulses to a full-width-half-maximum (FWHM) focal spot of 5 μm in diameter, containing 30% of the total laser energy (about 1.8 J), and corresponding to intensity of $\sim 8.3\times10^{19}$ W/cm^2. The p polarized pulses are incident onto different targets (aluminum or plastic) with various thicknesses at 30° with respect to the target normal. A cross-polarized wave (XPW) [30] filter was introduced to enhance the intensity contrast to a ratio of 10^{-10} at 40 ps prior to the peak of laser intensity. Figure 1 (top-left) is the schematic of the experiment setup. A Thomson parabola spectrometer (TPS) located at the back of the targets with an acceptance angle of 1.6 μSr was applied to record the spectra of protons. A multi-channel plate with a phosphor screen and a 16-bit electron multiplying charged-coupled device were used to enhance the parabolic ion traces. In addition, energy-resolved spatial distributions of proton beams were also recorded by an attached radiochromic files (RCF) stacks [31].

Experimental results Figure 1(a) displays the cut-off

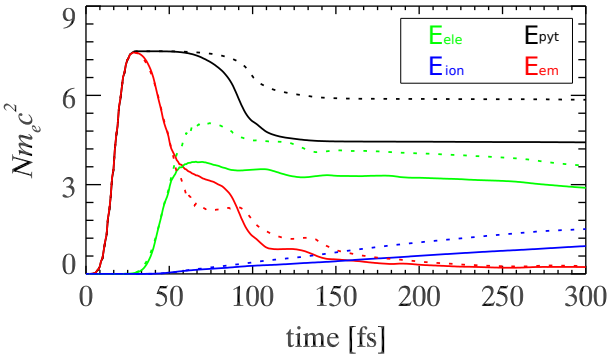

FIG. 2. (color online) The energy (transfer) as a function of time. Data are shown for laser energy entering into the simulation box (black), electromagnetic energy (red), electron kinetic energy (green) and ion kinetic energy (blue). The results from plastic targets (dashed lines) are compared with those from aluminum targets (solid lines). Here, the thickness is 1.2 μm for both aluminum and plastic targets.

energies of protons as a function of target thickness, where the laser parameters and target materials are fixed, and the values of cut-off energies are obtained by averaging over the 5 best shorts for each target with same thickness. Fig. 1(b) shows the optimum proton spectra obtained for the two types of targets. As seen from the figure, the aluminum target appears an optimal thickness at 2.5 μm. For target with thinner thickness, it is easily broken or distorted by the laser pre-pulse, significantly preventing the acceleration process. In contrast, for a thicker target above the optimal thickness, the reduced cut-off energy is found. Similar trend is shown for plastic

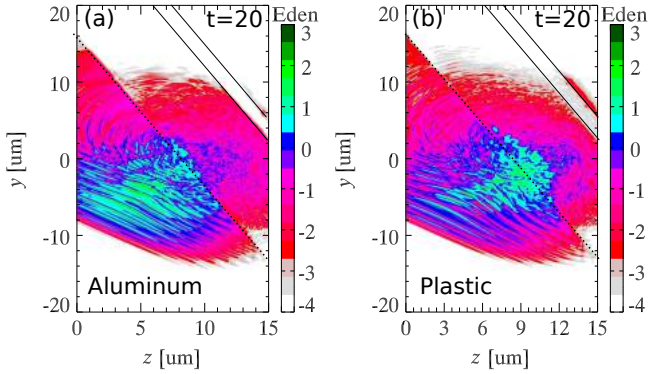

FIG. 3. (color online) (a)-(b) Electromagnetic energy densities for aluminum and plastic targets at $t = 53$ fs (i.e., $20T_0$). The solid lines indicate the initial positions of the solid targets and the dashed lines mark the fronts of preplasma. The thickness is 1.2 μm for both targets.

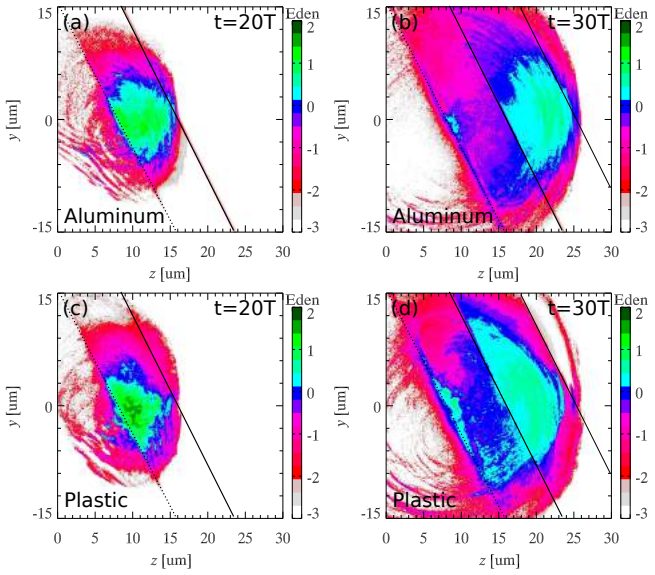

FIG. 4. (color online) (a)-(b) and (c)-(d), the kinetic energy distributions of the electrons for the aluminum and plastic targets with same thickness of 8 μm, at $t = 53$ fs (i.e., $20T_0$) and $t = 80$ fs (i.e., $30T_0$).

targets, although the exact optimum thickness maybe has not be scanned yet due to the thickness gap between 2 μm and 8 μm thickness (limited by the target making technology). Nevertheless, for a large range of target thickness, the cut-off energies from plastic targets are always much higher than that from aluminum. The optimal cut-off energy are 9.5 MeV and 13.5 MeV for aluminum and plastic targets, as shown in Fig. 1(b). It is also note that the total charge of the proton from the plastic target is significantly higher than that from the aluminum, with a 2.9 times increase in terms of the total energy (integral of the spectra in Fig. 1(b)). Furthermore, in Fig. 1(c)-1(h), energy-resolved spatial distributions of protons are presented for 2.5 μm aluminum and 1.2 μm plastic targets, respectively. The latter has a larger beam spot. By collecting the above experimental data, we can therefore draw the following conclusions: a) total charge and cut-off energies from plastic targets are higher than that from aluminum targets; b) uniformity of proton beam from plastic targets are better than that from aluminum targets; Although conclusion a) was already reported in existing studies [11, 12], and conclusion b) is also consistent with existing work [14–16], previous interpretations are successful in explaining each single aspect.

Simulation setups In order to analyse the experiments, we carried out numerical simulations with the PIC code LAPINS [26, 32, 33]. This code is based on a high order implicit numerical scheme, and takes advantage of the newly developed ionization and collision dynamics models. This code enables us to calculate coupled atomic and plasma processes for solid density targets in a more realistic way. Although with improved laser contrast by the XPW, we still need to deal with the pre-plasma expansion caused by ps lasting pre-pulse carefully. By performing radiation hydrodynamic simulation, the expansion caused by the ps pre-pluse is calculated. A small region of pre-plasma with sharp gradient 0.1 μm is formed. In the following PIC simulation, the target is modelled as a uniform slab with the pre-plasma. In order to figure out the effects of material property, aluminum (density of 2.7 g/cm^3) and plastic (density of 1.186 g/cm^3 with C:H:O=5:8:s2) target with same thickness (several micrometers) and fixed pre-plasmas are applied. The simulations were carried out in the Z-Y Cartesian geometry. The size of the box is chosen to be Z (40 μm)×Y (40 μm), which is divided into 2000×2000 uniform grids. The contamination is modelled as a hydrogen layer with thickness of 0.1 μm and density of 10^{21}/cm^3 on the backside for both aluminum and plastic targets, respectively. The initial temperature of the solid targets is chosen to be 0.1 eV. The initial ionization degree is set at $Z = 3$ for aluminum and $Z = 0$ for plastic. Afterward, the ionization is fully determined by the competition between field ionization, collision ionization and recombinations. The p polarized laser pulse is irradiated on the target with a fixed angle of 30 degree with respect to the target normal. The laser pulse has a predefined profile of form $\exp(-r^2/r_0^2)\sin^2(\pi t/2\tau_0)$, with $r_0 = 3\lambda_0$, $\tau_0 = 5T_0$ where T_0 is the laser cycle. The central wavelength of the laser is 0.8 μm and the normalized amplitude $a = eE/m_e\omega_0 c = 8$, where $\omega_0 = 2\pi/T_0$. In the Z and Y directions, absorbing boundary conditions are applied for both particles and laser field.

Simulation results Figure 2 shows the temporal evolution of energy (transfer) into the simulation box, including laser energy entering (black), electromagnetic field energy (red), electron kinetic energy (green), and the ion kinetic energy (blue), which are represented by $E_{\rm pyt}$, $E_{\rm em}$, $E_{\rm ele}$ and $E_{\rm ion}$, repetitively. Based on their time evolution, we obtain further insights into the whole laser solid interaction processes. The laser energy enters into the simulation box is calculated as $E_{\rm pyt} = \sum(E \times B)\delta y \delta t$,

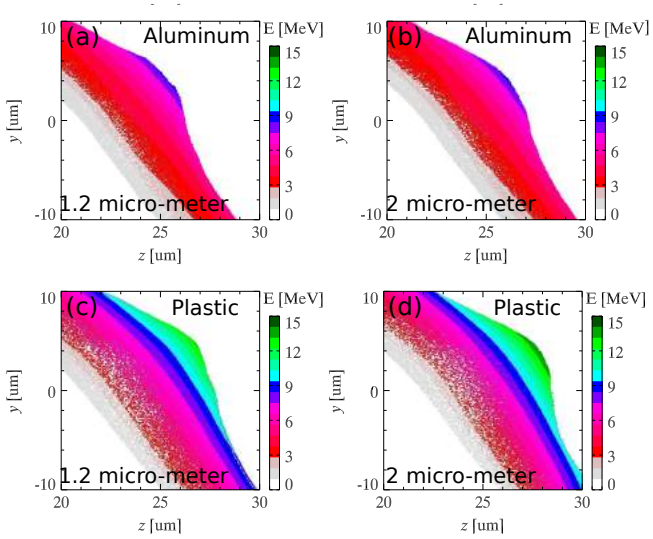

FIG. 5. (color online) The spatial distribution of proton energies for the aluminum and plastic targets, at $t = 320$ fs (i.e., $120T_0$), respectively.

where δt is the time step of the simulation box. $E_{\rm pyt}$ first increases and arrives at a constant value at $t = 25$ fs, when the whole laser is entirely injected into the simulation box. Afterward till $t = 75$ fs, we find that there is a strong energy transfer from the electromagnetic energy $E_{\rm em}$ to the electron-kinetic energy $E_{\rm ele}$ and then to the ion-kinetic energy $E_{\rm ion}$, and to which we briefly refer as the laser plasma interaction stage in front of the target. In this stage, the efficiency for coupling the energy from laser to plastic is significantly higher than to aluminum. At $t = 75$ fs, $E_{\rm pyt}$ starts to decrease, meaning the reflected laser is leaving the simulation box. The quicker drop of $E_{\rm pyt}$ shows the reflection ratio of the aluminum is significantly higher than for the plastic. After $t = 100$ fs, when the main body of the laser pulse is reflected back, we can still notice a gradual energy transfer from electrons to ions, which is referred to as the thermal expansion stage and target normal sheath acceleration.

In Fig. 3, the electromagnetic energy densities are presented for both aluminum and plastic targets with thickness of 1.2 μm. The snapshot is taken at $t = 53$ fs–a typical time within the laser plasma interaction window (from $t = 25$ fs to $t = 75$ fs). It appears that the penetration depth within the plastic is larger than of aluminum. A deeper penetration will significantly enhance efficiency of energy transfer from laser to plasmas, through various mechanisms [36–38], typically including $\mathbf{J} \times \mathbf{B}$ mechanism, vacuum heating, direct laser accelerations. The possible reason is the lower electron density for fully ionized plastic than that of aluminum.

Figure 4 presents the kinetic energy densities of electrons, indicating the transport process of hot electrons within the solids. Although breakdown of plastic might happen by the pre-pulse (currently beyond the capabilities of radiation hydrodynamic simulations), as an initial insulator, the resistivity of plastic target is very large compared with aluminum target. According to the Ohm's law $\boldsymbol{E} = \eta \boldsymbol{J}_e$, where η is the resistivity of the bulk target and $\boldsymbol{J}_e$ is the current density of electrons, an intense resistive electric field will inhibit the transport of hot electrons. As shown in Fig. 4, when compared with aluminum targets [See Fig. 4(a) and (b)], the inhibition and deflection of hot electron transport in plastic targets [See Fig. 4(c) and (d)] lead to a larger hot electron spot. The divergent transport of hot electrons will lead to a larger spatial spot of accelerated proton beams, since they are mainly accelerated by the expansion of hot electrons on the backside of the target. Moreover, we found the electron energy density is significantly decreased during the transport in both aluminum and plastic target. This is due to the energy deposition and energy losses of hot electrons during transport. By further increasing target thickness, the cut-off energies of protons will accordingly decreased.

In Fig. 5, the spatial energy distribution of proton for aluminum and plastic targets are presented at 320 fs, the end of simulation when acceleration reaches saturations. Compared with Fig. 1, remarkable agreement is found between simulation and experiment on both energies and spot uniformity. Please note that the energetic protons are from the rear contamination at the back surface for both types of target. This is different from the existing work [11–13] which assume protons are accelerated by the resistive electric field for plastic targets. Our research indicate that the energy conversion efficiency determined by the target material properties is the key parameter.

Conclusions To summarize, we report experimental and numerical simulation investigations of laser-driven proton accelerations under two solid materials: aluminum as a typical conductor and plastic as a typical insulator. Significant effects of target materials are found on the total charge, cut-off energies and beam spot sizes of protons. Generally the plastic target produces proton beams with higher charge, larger cut-off energy, and better beam uniformity than the aluminum target under the same thickness with same laser conditions. Two dimensional particle-in-cell simulations well elucidate the dependence of the target material on the laser-driven acceleration of protons by including both ionization dynamics and collision dynamics. This work indicate that the simulation should probably better use laser-solid interaction models instead of pure laser-plasma interaction in order to be closer to the experiment.

ACKNOWLEDGMENTS

This work was supported by National Natural Science Foundation of China (No. 11605269, 11721091, 11775144 and 11475010), ITER-CHINA Program (No. 2015GB120001), National Grand Instrument Project (No. 2012YQ030142) and Science Challenge Project (No. TZ2016005).

[1] S. C. Wilks, A. B. Langdon, T. E. Cowan, M. Roth, M. Singh, S. Hatchett, M. H. Key, D. Pennington, A. MacKinnon, and R. A. Snavely, Phys. Plasmas 8, 542 (2001).

[2] L. Yin, B. J. Albright, K. J. Bowers, D. Jung, J. C. Fernandez, and B. M. Hegelich, Phys. Rev. Lett. 107, 045003 (2011).

[3] D. Haberberger, S. Tochitsky, F. Fiuza, C. Gong, R. A. Fonseca, L. O. Silva, W. B. Mori, and C. Joshi, Nat. Phys. 8, 95 (2012).

[4] H. Daido, M. Nishiuchi, and A. S. Pirozhkov, Rep. Prog. Phys. 75, 056401 (2012).

[5] C. Wang, X.-T. He, and P. Zhang, Phys. Rev. Lett. 106, 145002 (2011).

[6] C. K. Li, F. H. S guin, J. R. Rygg, J. A. Frenje, M. Manuel, R. D. Petrasso, R. Betti, J. Deletetrez, J. P. Knauer, F. Marshall, D. D. Meyerhofer, D. Shvarts, V. A. Smalyuk, C. Stoeckl, O. L. Landen, R. P. J. Town, C. A. Back, and J. D. Kilkenny, Phys. Rev. Lett. 100, 225001 (2008).

[7] M. Roth, T. E. Cowan, M. H. Key, S. P. Hatchett, C. Brown, W. Fountain, J. Johnson, D. M. Pennington, R. A. Snavely, S. C. Wilks, K. Yasuike, H. Ruhl, F. Pegoraro, S. V. Bulanov, E. M. Campbell, M. D. Perry, and H. Powell, Phys. Rev. Lett. 86, 436 (2001).

[8] R. A. Snavely, M. H. Key, S. P. Hatchett, T. E. Cowan, M. Roth, T. W. Phillips, M. A. Stoyer, E. A. Henry, T. C. Sangster, M. S. Singh, S. C. Wilks, A. MacKinnon, A. Offenberger, D. M. Pennington, K. Yasuike, A. B. Langdon, B. F. Lasinski, J. Johnson, M. D. Perry, and E. M. Campbell, Phys. Rev. Lett. 85, 2945 (2000).

[9] T. Z. Esirkepov, S. V. Bulanov, K. Nishihara, T. Tajima, F. Pegoraro, V. S. Khoroshkov, K. Mima, H. Daido, Y. Kato, Y. Kitagawa, K. Nagai, and S. Sakabe, Phys. Rev. Lett. 89, 175003 (2002).

[10] M. Borghesi, J. Fuchs, S. V. Bulanov, A. J. MacKinnon, P. K. Patel, and M. Roth, Fusion Sci. Technol. 49, 412 (2006).

[11] K. Lee, S. H. Park, Y.-H. Cha, J. Y. Lee, Y. W. Lee, K.-H. Yea, and Y. U. Jeong, Phys. Rev. E 78, 056403.

[12] K. Lee, J. Y. Lee, S. H. Park, Y.-H. Cha, Y. W. Lee, K. N. Kim, and Y. U. Jeong, Phys. Plasmas 18 013101 (2011).

[13] A. Macchi, M. Borghesi, and M. Passoni, Rev. Mod. Phys. 85, 751 (2013).

[14] F. Pisani, A. Bernardinello, D. Batani, A. Antonicci, E. Martinolli, M. Koenig, L. Gremillet, F. Amiranoff, S. Baton, J. Davies, T. Hall, D. Scott, P. Norreys, A. Djaoui, C. Rousseaux, P. Fews, H. Bandulet, and H. Pepin Phys. Rev. E 62, R5927(R) (2000).

[15] J. Fuchs, T. E. Cowan, P. Audebert, H. Ruhl, L. Gremillet, A. Kemp, M. Allen, A. Blazevic, J.-C. Gauthier, M. Geissel, M. Hegelich, S. Karsch, P. Parks, M. Roth, Y. Sentoku, R. Stephens, and E. M. Campbell, Phys. Rev. Lett. 91, 255002 (2003).

[16] P. Gibbon, Phys. Rev. E 72, 026411 (2005).

[17] A. J. Kemp, R. E. W. Pfund, and J. Meyer-ter-Vehn, Phys. Plasmas 11, 5648 (2004).

[18] M. V. Ammosov, N. B. Delone, and V. P. Krainov, Sov. Phys. JETP 64, 1191 (1986).

[19] K. Nanbu, S. Yonemura, J. Comput. Phys. 145, 639 (1998).

[20] Y. Sentoku, A. J. Kemp, J. Comput. Phys. 227, 6846 (2008).

[21] S. M. Vinko, O. Ciricosta, T.R. Preston, D.S. Rackstraw, C.R.D. Brown, T. Burian, J. Chalupsky, et alB.I. Cho, H.-K. Chung, K. Engelhorn, R.W. Falcone, R. Fiokovinini, V. Hajkova, P.A. Heimann, L. Juha, et al H.J. Lee, R.W. Lee, M. Messerschmidt, B. Nagler, W. Schlotter, J.J. Turner, L. Vysin, U. Zastrau, and J.S. Wark, Nat. Commun. 6, 6397 (2015).

[22] S. M. Vinko, O. Ciricosta, B. I. Cho, K. Engelhorn, H.-K. Chung, C. R. D. Brown, T. Burian, J. Chalupsky, R. W. Falcone, C. Graves, V. Hájková, A. Higginbotham, L. Juha, J. Krzywinski, H. J. Lee, M. Messerschmidt, C. D. Murphy, Y. Ping, A. Scherz, W. Schlotter, S. Toleikis, J. J. Turner, L. Vysin, T. Wang, B. Wu, U. Zastrau, D. Zhu, R. W. Lee, P. A. Heimann, B. Nagler and J. S. Wark, Nature, 482, 59 (2012).

[23] P. Leblanc and Y. Sentoku, Phys. Rev. E 89, 023109 (2014).

[24] Y. Sentoku, E. dHumieres, L. Romagnani, P. Audebert, and J. Fuchs, Phys. Rev. Lett. 107, 135005 (2011).

[25] L. G. Huang , T. Kluge, and T. E. Cowan, Phys. Plasmas 23, 063112 (2016).

[26] D. Wu, X. T. He, W. Yu and S. Fritzsche, Phys. Rev. E 100, 013207 (2019).

[27] D. Wu, X. T. He, W. Yu, and S. Fritzsche, Phys. Rev. E 95, 023208 (2017).

[28] D. Wu, B. Qiao, C. McGuffey, X. T. He, and F. N. Beg, Phys. Plasmas 21, 123118 (2014).

[29] D. Wu, X. T. He, W. Yu, and S. Fritzsche, Phys. Rev. E 95, 023207 (2017).

[30] A. Jullien, J.-P. Rousseau, B. Mercier, L. Antonucci, O. Albert, G. Chériaux, S. Kourtev, N. Minkovski, and S. M. Saltiel, Opt. Lett. 33, 2353 (2008).

[31] F. Nurnberg, M. Schollmeier, E. Brambrink, A. Blazevic, D. Carroll, K. Flippo, D. Gautier, M. Geissel, K. Harres, B. Hegelich, et al, Rev. Sci. Instrum. 80, 033301 (2009).

[32] D. Wu, X. T. He, W. Yu and S. Fritzsche, High Power Laser Science and Engineering, 6, e50 (2018).

[33] D. Wu, W. Yu, Y. T. Zhao, D. H. H. Hoffmann, S. Fritzsche, and X. T. He, Phys. Rev. E 100, 013208 (2019).

[34] H. Xu, W. W. Chang, H. B. Zhuo, L. H. Cao, and Z. W. Yue, Chin. J. Comput. Phys. 19, 305 (2002).

[35] A. Sunahara, T. Johzaki, H. Nagatomo, and K. Mima, Laser and Particle Beams 30, 95 (2012).

[36] B. S. Paradkar, S. I. Krasheninnikov, and F. N. Beg, Phys. Plasmas 19, 060703 (2012).

[37] A. Sorokovikova, A. V. Arefiev, C. McGuffey, B. Qiao, A. P. L. Robinson, M. S. Wei, H. S. McLean, and F. N. Beg, Phys. Rev. Lett. 116, 155001 (2016).

[38] D. Wu, S. I. Krasheninnikov, S. X. Luan, and W. Yu, Nucl. Fusion 57, 016007 (2017).